Earth and Planetary Science Letters 390 (2014) 199–208

Contents lists available at ScienceDirect

Earth and Planetary Science Letters

www.elsevier.com/locate/epsl

Experimental constraints on Mercury's core composition

Nancy L. Chabot [a,*], E. Alex Wollack [b], Rachel L. Klima [a], Michelle E. Minitti [a]

[a] The Johns Hopkins University Applied Physics Laboratory, Laurel, MD 20723, USA
[b] Princeton University, Princeton, NJ 08540, USA

ARTICLE INFO

Article history:
Received 10 June 2013
Received in revised form 13 November 2013
Accepted 6 January 2014
Available online 31 January 2014
Editor: T. Elliott

Keywords:
Mercury
core formation
metal–silicate partitioning
Fe–S–Si
sulfur

ABSTRACT

The recent discovery of high S concentrations on the surface of Mercury by spacecraft measurements from the MESSENGER mission provides the potential to place new constraints on the composition of Mercury's large metallic core. In this work, we conducted a set of systematic equilibrium metal–silicate experiments that determined the effect of different metallic compositions in the Fe–S–Si system on the S concentration in the coexisting silicate melt. We find that metallic melts with a range of S and Si combinations can be in equilibrium with silicate melts with S contents consistent with Mercury's surface, but that such silicate melts contain Fe contents lower than measured for Mercury's surface. If Mercury's surface S abundance is representative of the planet's bulk silicate composition and if the planet experienced metal–silicate equilibrium during planetary core formation, then these results place boundaries on the range of possible combinations of Si and S that could be present as the light elements in Mercury's core and suggest that Mercury's core likely contains Si. Except for core compositions with extreme abundances of Si, bulk Mercury compositions calculated by using the newly determined range of potential S and Si core compositions do not resemble primitive meteorite compositions.

1. Introduction

Mercury is a planet of extremes. It is the smallest, the closest to the Sun, and also the densest when the uncompressed density is considered. Mercury's high density (Anderson et al., 1987) indicates the presence of a large metallic core that comprises roughly two-thirds of the planet, a much larger fraction than the other terrestrial planets of Venus, Earth, or Mars (Goettel, 1988). Additionally, Earth-based radar measurements showed that Mercury's core is at least partially molten (Margot et al., 2007). Earth-based and spacecraft spectral observations of Mercury's surface indicated the surface silicates are Fe-poor due to lack of absorption features, suggesting $< \sim$3% FeO in the surface silicates (Blewett et al., 1997; McClintock et al., 2008; Robinson and Taylor, 2001; Vilas, 1988).

In March 2011, the MESSENGER (MErcury Surface, Space ENvironment, GEochemistry, and Ranging) spacecraft became the first ever to orbit Mercury, and as such is providing a wealth of new data about the Solar System's innermost planet (Bedini et al., 2012). In particular, MESSENGER's X-ray and gamma-ray spectrometers have yielded the first measurements of the elemental composition of Mercury's surface (Evans et al., 2012; Nittler et al., 2011; Peplowski et al., 2011, 2012a, 2012b; Starr et al., 2012; Weider et al., 2012). The composition shows variability across the surface, and for Fe and S, two elements pertinent to our study, Mercury's surface ranges from roughly 1–4 wt% for both the Fe and S content (Evans et al., 2012; Nittler et al., 2011; Starr et al., 2012; Weider et al., 2012). There is general agreement between the X-ray and gamma-ray results, which sample the top $\sim$100 μm (Weider et al., 2012) and $\sim$tens of centimeters (Evans et al., 2012) of the surface respectively, suggesting that Mercury's regolith is homogeneous to at least a depth of $\sim$tens of centimeters. Based on the measured surface Fe and S contents, the oxygen fugacity of Mercury's interior is quite reducing, with estimates ranging from -2.6 to -7.3 in log units relative to the iron–wüstite buffer (McCubbin et al., 2012; Zolotov et al., 2013).

MESSENGER's gravity data have also provided additional insight into Mercury's internal structure. The results suggest that the depth to Mercury's liquid core is $\sim$400 km (Smith et al., 2012). Additionally, the first models of Mercury's solid layer above the liquid core suggested a higher density than that expected for Fe-poor silicates; this led to the proposal that a solid layer of FeS could be buoyantly stable at the top of the metallic core and thus provide a higher density solid material at the base of the mantle to explain the MESSENGER gravity measurements (Smith et al., 2012). Based on Mercury's reduced conditions, Malavergne et al. (2010) had previously suggested the possibility of Mercury's core containing both S and Si, and explored a variety of core crystallization scenarios that could arise, including the formation of a buoyant solid FeS layer. Chen et al. (2008) and Riner et al. (2008) also examined a variety of crystallization and layered core scenarios for Mercury in the Si-free Fe–S system, which were dependent on Mercury's unknown core S composition. Utilizing the latest determinations of

* Corresponding author. Tel.: +1 240 228 5558; fax: +1 240 228 8939.
E-mail address: Nancy.Chabot@jhuapl.edu (N.L. Chabot).

0012-821X/$ – see front matter
http://dx.doi.org/10.1016/j.epsl.2014.01.004

Mercury's gravity field and Earth-based radar observations of the planet's spin state, Hauck et al. (2013) modeled Mercury's internal structure and considered core compositions in the Fe–S–Si system, including scenarios with a solid FeS layer at the top of the core.

Enstatite chondrites are primitive meteorites with Fe-poor silicates, suggesting their formation in highly-reduced conditions (Keil, 1989) and therefore their potential applicability as analog material for understanding Mercury's evolution. Partial melting experimental studies that used the Indarch enstatite chondrite as the starting composition created multiple sulfides, Fe-poor silicates, S-bearing silicate melts, and Si-bearing metals (Berthet et al., 2009; McCoy et al., 1999); these enstatite chondrite melting experiments thus offer intriguing potential for implications to Mercury's surface, given in particular the high S content of ∼1–4 wt% from MESSENGER measurements. Metal–silicate partitioning experiments with applications for Earth's core formation concluded that S and Si were mutually exclusive in the metal phase, as the reducing conditions required to put Si in the metallic core would cause S to partition into the silicate melt (Kilburn and Wood, 1997), raising the question of whether Mercury's core could contain both S and Si. Other metal–silicate experimental studies have explored the partitioning behavior of S under a variety of pressure, temperature, oxygen fugacity, and composition conditions (Holzheid and Grove, 2002; Li and Agee, 2001; Rose-Weston et al., 2009). These previous experimental studies naturally were focused on conditions relevant to Earth, rather than the highly-reduced conditions experienced on Mercury, given the lack of chemical data for Mercury prior to MESSENGER's orbital measurements.

In this work, we conduct a set of systematic metal–silicate partitioning experiments designed to examine the effect that different metallic compositions in the Fe–S–Si system would have on the coexisting silicate. For Mercury, we have measurements of the planet's silicate surface, so we examine what constraints the chemical signatures measured in the silicate can provide on the composition of Mercury's large metallic core.

2. Methods

All experiments were conducted at 1 atm and 1500 °C in a vertical tube Deltech furnace at the Johns Hopkins University Applied Physics Laboratory using evacuated and sealed silica glass tubes, a technique well-established in previous experimental studies in this lab (Chabot et al., 2010, 2009, 2007).

To systematically examine the effect of varying the metallic composition of Mercury's core, we have restricted our experiments to a single starting silicate composition. This starting composition was based on measurements reported from the MESSENGER spacecraft for the major element surface composition of Mercury (Evans et al., 2012; Nittler et al., 2011; Starr et al., 2012; Weider et al., 2012). Ideally, these metal–silicate partitioning experiments would be conducted with a silicate composition that was representative of Mercury's bulk silicate composition, but the composition of Mercury's mantle is poorly constrained. The starting silicate was produced by mixing commercially purchased powders of SiO_2, $CaCO_3$, Al_2O_3, MgO, and TiO_2 (Table A1) and then decarbonating the mixture at 900 °C for 1 hour prior to the experiments.

The starting metallic material was varied between the experiments and was a mixture of Fe, FeS, and Si commercially purchased powders (Table A2). The different metallic compositions also resulted in different oxygen fugacity conditions between the runs. Starting silicate and metallic materials were mixed in a roughly 1:2 weight ratio and placed into a hard alumina crucible with an outer diameter of 6.5 mm and a wall thickness of 1.1 mm. The crucible was inserted in a high purity silica tube, with an outer diameter of 12 mm and a wall thickness of 2.1 mm. The tube was evacuated and then sealed while under vacuum. The evacuated tube was lowered into the Deltech vertical tube furnace and held at 1500 °C for ∼4 hours. Tubes were then removed from the furnace and quenched in a water bath. The alumina crucible was removed from the tube, mounted in epoxy, and sliced with a diamond saw to expose a cross-section of the experiment. The cross section was mount in epoxy and polished with alumina powder in preparation for analysis.

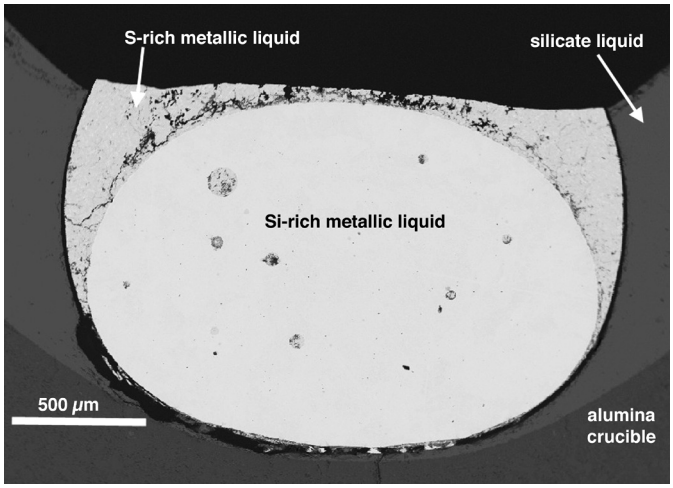

Fig. 1. Back-scattered electron image of experimental run #M1. The silicate was liquid at run conditions and quenched to a glass. In this experiment, two immiscible metallic liquids were present at run conditions, one S-rich and one Si-rich, which exhibit multi-phase textures upon quenching.

Run products consisted of quenched silicate and metallic phases that had been liquid at run conditions. Fig. 1 shows a back-scattered electron image of a typical run product. The silicate liquid quenched to a predominantly glass phase in all experiments. The runs either had one or two metallic liquids, depending on the bulk composition of the metal and whether liquid immiscibility was encountered in the Fe–S–Si system (Raghavan, 1988). If the run encountered the liquid immiscibility field in the Fe–S–Si system, two metallic liquids were present, one S-rich and one Si-rich. Sulfur-rich metallic liquids had a typical dendritic quench texture of Fe dendrites surrounded by predominantly interstitial FeS. Silicon-rich metallic liquids also displayed quench texture but it was more subdued, as reported in previous Fe–S–Si experiments (Chabot et al., 2010).

All experiments were analyzed on a JEOL JSM-6500F field emission scanning electron microscope at the Carnegie Institution of Washington, with settings of 15 kV, 1 nA, and 30 s acquisition time. Standards used were Fe_3O_4, MgO, Al_2O_3, SiO_2, FeS_2, Fe, wollastonite, diopside, orthoclase, and a natural basalt. Analyses were conducted such as to sample rectangular areas between 100 and 200 μm on a side, enabling the bulk composition of phases with quench textures to be determined. At least three measurements were made of each phase and averaged to determine the composition, with errors determined as the standard deviation of the multiple analyses.

3. Results

Tables 1 and 2 summarize the final compositions of the silicate and metallic phases. Five runs with the same starting metallic composition were conducted for durations of 0.5, 1, 2 (#M31), 4 (#M1), and 16 (#M34) hours. The three experiments with durations $\geqslant$2 hours produced run products with consistent silicate and metallic compositions, as reported in Tables 1 and 2. In contrast, the two experiments with durations $\leqslant$1 hour resulted in silicate compositions with slightly higher Si contents (∼23 wt%) and

Table 1
Final silicate melt compositions of experiments (wt%).

Run #	Hours	Si	Ti	Al	Fe	Mg	Ca	S	O	Total
M1	4	18.9 ± 0.1	0.32 ± 0.02	17.3 ± 0.2	0.28 ± 0.04	8.4 ± 0.1	6.0 ± 0.1	3.1 ± 0.1	44.6 ± 0.5	98.9
M5	3.5	14.4 ± 0.1	0.37 ± 0.02	9.7 ± 0.2	25.4 ± 0.6	7.4 ± 0.1	4.5 ± 0.1	0.5 ± 0.1	40.3 ± 0.4	102.5
M10	4	16.9 ± 0.2		19.9 ± 0.3	0.51 ± 0.05	9.3 ± 0.2	4.4 ± 0.1	8.6 ± 0.1	41.8 ± 1.1	101.4
M12	4	20.5 ± 0.1	0.31 ± 0.02	19.2 ± 0.5	0.30 ± 0.07	7.9 ± 0.1	4.5 ± 0.1	1.2 ± 0.1	46.3 ± 0.4	100.2
M13	4	19.4 ± 0.1	0.33 ± 0.06	19.4 ± 0.1	0.12 ± 0.05	8.1 ± 0.1	5.6 ± 0.1	3.2 ± 0.1	44.6 ± 0.1	100.7
M14	4	18.0 ± 0.2	0.28 ± 0.05	14.9 ± 0.2	13.5 ± 0.3	7.3 ± 0.1	4.3 ± 0.1	0.09 ± 0.02	45.2 ± 0.5	103.6
M17	4.5	19.8 ± 0.1	0.34 ± 0.05	18.2 ± 0.2	0.21 ± 0.05	8.6 ± 0.1	5.9 ± 0.1	2.6 ± 0.1	45.0 ± 0.3	100.6
M19	4	20.1 ± 0.1	0.26 ± 0.02	18.8 ± 0.2	0.25 ± 0.04	7.8 ± 0.1	5.9 ± 0.1	1.5 ± 0.1	45.7 ± 0.3	100.2
M20	4.5	19.3 ± 0.1	0.31 ± 0.03	19.1 ± 0.3	0.11 ± 0.06	8.5 ± 0.1	5.8 ± 0.1	3.2 ± 0.1	45.4 ± 0.6	101.6
M26	6	18.6 ± 0.1		20.3 ± 0.2	0.29 ± 0.02	8.6 ± 0.1	5.1 ± 0.1	5.0 ± 0.1	45.0 ± 0.5	102.9
M27	6	20.0 ± 0.3		17.9 ± 0.2	0.24 ± 0.09	8.7 ± 0.1	5.8 ± 0.1	1.6 ± 0.1	47.8 ± 0.3	102.0
M31	2	19.3 ± 0.2	0.13 ± 0.05	17.8 ± 0.4	0.25 ± 0.05	9.8 ± 0.1	5.3 ± 0.1	3.8 ± 0.1	46.2 ± 0.8	102.5
M33	5	20.0 ± 0.1	0.37 ± 0.04	18.9 ± 0.2	0.11 ± 0.03	8.3 ± 0.1	5.6 ± 0.1	2.1 ± 0.1	47.0 ± 0.3	102.2
M34	16	18.4 ± 0.2		19.4 ± 0.3	0.23 ± 0.04	7.8 ± 0.1	6.2 ± 0.1	4.1 ± 0.1	45.6 ± 1.1	101.8
M35	4	19.7 ± 0.3	0.47 ± 0.02	16.8 ± 0.5	0.4 ± 0.2	9.3 ± 0.1	6.3 ± 0.1	1.8 ± 0.1	47.5 ± 1.3	102.3
M36	4	18.1 ± 0.2	0.30 ± 0.05	19.6 ± 0.2	0.13 ± 0.04	9.1 ± 0.1	5.0 ± 0.1	5.6 ± 0.1	44.8 ± 0.5	102.6
M37	4	17.3 ± 0.3	0.41 ± 0.07	14.2 ± 0.2	14.3 ± 0.2	7.0 ± 0.1	4.3 ± 0.1	0.19 ± 0.02	45.4 ± 0.8	103.1
M38	4.5	19.4 ± 0.1	0.26 ± 0.01	18.7 ± 0.1	0.06 ± 0.03	8.6 ± 0.1	5.7 ± 0.1	3.1 ± 0.1	46.6 ± 0.1	102.3
M40	4.5	17.1 ± 0.2		19.9 ± 0.3	0.39 ± 0.05	9.7 ± 0.1	4.5 ± 0.1	7.6 ± 0.1	42.9 ± 0.8	102.2

All errors are ±1 standard deviation.

Table 2
Final metal compositions of the experiments (wt%) and calculated metal–silicate partition coefficient, $D(S)$.

Run #	S	Si	Ti	Fe	Total	$D(S)$
M1 – S	31.9 ± 0.5		1.9 ± 0.1	63.0 ± 0.8	96.8	10.3 ± 0.4
M1 – Si	1.5 ± 0.1	7.7 ± 0.1		88.4 ± 0.6	97.6	0.48 ± 0.04
M1 – bulk[a]	7.0 ± 0.2	6.3 ± 0.1		83.8 ± 0.7	97.1	2.3 ± 0.1
M5	20.1 ± 1.4			79.0 ± 1.1	99.1	40 ± 9
M10 – S	35.2 ± 0.5		1.7 ± 0.1	60.0 ± 0.7	96.8	4.1 ± 0.1
M10 – Si	0.66 ± 0.03	13.4 ± 0.1		85.5 ± 0.3	99.5	0.08 ± 0.01
M10 – bulk[a]	10.6 ± 0.2	9.5 ± 0.1		78.1 ± 0.4	98.3	1.23 ± 0.02
M12	5.1 ± 0.8	5.1 ± 0.2		90.1 ± 0.5	100.4	4.3 ± 0.8
M13	1.1 ± 0.1	12.4 ± 0.1		88.8 ± 0.7	102.8	0.34 ± 0.03
M14	6.9 ± 0.6			95.9 ± 0.6	102.8	80 ± 20
M17 – S	32.0 ± 0.4	0.3 ± 0.1	0.7 ± 0.4	65.4 ± 1.3	98.3	12.3 ± 0.5
M17 – Si	2.2 ± 0.1	7.4 ± 0.1		80.3 ± 0.9	99.8	0.85 ± 0.05
M17 – bulk[a]	3.7 ± 0.1	7.0 ± 0.1		89.9 ± 0.9	99.7	1.4 ± 0.1
M19 – S	31.6 ± 1.4		0.4 ± 0.1	67.3 ± 0.9	101.3	21 ± 2
M19 – Si	3.1 ± 0.1	4.5 ± 0.1		92.9 ± 0.6	100.4	2.1 ± 0.2
M19 – bulk[a]	9.5 ± 0.4	3.5 ± 0.1		87.1 ± 0.7	100.1	6.3 ± 0.5
M20	0.7 ± 0.1	13.3 ± 0.1		87.4 ± 0.2	101.4	0.22 ± 0.03
M26 – S	32.8 ± 0.4		0.8 ± 0.1	62.4 ± 0.3	96.0	6.6 ± 0.2
M26 – Si	1.0 ± 0.1	10.3 ± 0.2		87.7 ± 0.8	99.0	0.20 ± 0.02
M26 – bulk[a]	12.6 ± 0.2	6.5 ± 0.1		78.5 ± 0.6	97.7	2.5 ± 0.1
M27 – S	28.9 ± 0.6		0.3 ± 0.1	67.1 ± 1.5	96.2	18.1 ± 1.2
M27 – Si	3.6 ± 0.2	4.2 ± 0.1		90.8 ± 0.7	98.5	2.3 ± 0.2
M27 – bulk[a]	14.3 ± 0.4	2.4 ± 0.1		80.7 ± 1.0	97.4	8.9 ± 0.6
M31 – S	31.1 ± 0.9		0.4 ± 0.2	65.3 ± 0.3	96.7	8.2 ± 0.3
M31 – Si	3.2 ± 1.7	8.3 ± 0.4		87.4 ± 1.0	98.9	0.8 ± 0.5
M31 – bulk[a]	8.4 ± 1.6	6.8 ± 0.3		83.3 ± 0.9	98.5	2.2 ± 0.4
M33	0.5 ± 0.1	12.9 ± 0.2		85.9 ± 0.6	99.2	0.24 ± 0.05
M34 – S	32.9 ± 0.5		1.2 ± 0.3	60.3 ± 0.7	94.4	8.0 ± 0.2
M34 – Si	1.0 ± 0.1	9.8 ± 0.1		87.1 ± 1.1	97.9	0.24 ± 0.03
M34 – bulk[a]	7.9 ± 0.2	7.7 ± 0.1		81.4 ± 1.0	96.9	1.9 ± 0.1
M35	1.5 ± 0.1	8.1 ± 0.2		89.2 ± 1.5	98.8	0.8 ± 0.1
M36	0.4 ± 0.2	16.5 ± 0.2		82.0 ± 0.4	98.9	0.07 ± 0.04
M37	26.5 ± 0.7			72.8 ± 0.7	99.3	140 ± 20
M38	0.2 ± 0.1	16.9 ± 0.1		81.5 ± 0.1	98.6	0.06 ± 0.03
M40	0.8 ± 0.1	12.7 ± 0.1		85.4 ± 0.4	99.0	0.11 ± 0.01

All errors are ±1 standard deviation.
[a] Bulk compositions calculated by using mass balance calculations based on the starting Fe and S compositions, as detailed in Table A2 of the electronic supplement.

much lower S contents of <1 wt%, as compared to the ~3.5 wt% S consistently produced in the silicate of the longer duration runs with the same starting composition. Thus we conclude that by two hours, equilibrium partitioning for S and Si has been achieved in our experiments, and Tables 1 and 2 only report experiments with durations of ⩾2 hours.

As reported in Table 2, 8 of our 19 experiments encountered liquid immiscibility in the Fe–S–Si system and produced two metallic liquids. Comparison of the final metallic compositions in our experiments with the Fe–S–Si phase diagram (Raghavan, 1988) shows good agreement, as shown in Fig. A1 of the electronic supplement. Experiments that produced one metallic liquid have compositions that fall in the one liquid field, and the final compositions of metallic liquids in runs with two liquids are consistent with the liquid immiscibility field phase diagram. For the eight runs with two immiscible metallic liquids, the bulk metallic composition was also calculated. This was done by mass balance using the Fe and S concentrations in the starting material and the Fe and S

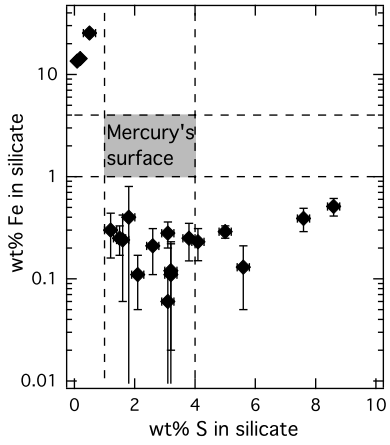

Fig. 2. The measured Fe and S contents of the silicate melt produced in our experiments are plotted. While many of the experiments produce S contents in the silicate that are consistent with those measured for Mercury's surface, none of the experiments also match Mercury's surface Fe content. Errors bars are two standard deviations.

concentrations measured in the final run product phases with the assumption of no loss during the experiments. The starting metallic compositions and the calculated percent mass of the silicate, S-rich metallic liquid, and Si-rich metallic liquid are given in Table A2 of the electronic supplement. The assumption of no loss during the experiments is an idealized scenario, as S can be lost to a vapor phase during the preparation or duration of the run. For the eight runs with two immiscible metallic liquids, the calculated percent mass values for the silicate, S-rich metallic liquid, and Si-rich metallic liquid were reasonable, with the final silicate phase representing about a third of the run product, consistent with the starting metal/silicate ratio. If S were lost during the run, the percent mass of the S-rich metal phase would be overestimated; in all eight runs, the S-rich metallic liquid was calculated to be the smallest percent mass phase, as listed on Table A2. The bulk metallic composition for these eight runs was calculated using these mass percentages and is reported in Table 2. Errors in the calculated bulk metallic composition were determined from the errors in each metallic phase weighted by the relative mass percentage contribution of that phase to the bulk metal.

3.1. Silicate composition

In Fig. 2, the Fe and S concentrations in the silicate produced in our experiments are compared to the 1–4 wt% Fe and 1–4 wt% S measured on Mercury's surface by MESSENGER investigations (Evans et al., 2012; Nittler et al., 2011; Starr et al., 2012; Weider et al., 2012). Some of our 19 experiments contain 1–4 wt% S in the silicate phase, but none of the runs also contain 1–4 wt% Fe; the Fe concentrations in our experiments that contain wt% levels of S in the silicate have Fe concentrations below 0.5 wt%. The low Fe concentrations in the silicate are generally consistent with previous work that shows that S solubility in a silicate melt increases as conditions become more reducing (Berthet et al., 2009; Haughton et al., 1974; Kilburn and Wood, 1997; Wallace and Carmichael, 1992). Recent calculations by Zolotov et al. (2013) also conclude that the oxygen fugacity conditions required to produce the S content observed on Mercury's surface would yield ~0.03–0.8 wt% FeO, and our experiments with 1–4 wt% S in the silicate fall within that range of Fe content in the silicate melt, as shown in Fig. 2.

That none of the silicates in our experiments are able to match both the Fe and S contents measured on Mercury's surface can mean many things. First, it could suggest that Mercury's Fe and S surface composition does not reflect a single molten melt–molten silicate differentiation event. This is undoubtedly true, as Mercury's surface shows extensive signs of volcanism and other geologic processes. How representative is Mercury's surface composition of Mercury's mantle and the planet's bulk silicate composition? This is an open question, and future geochemical studies based on MESSENGER's compositional results have the potential to provide important insight into this issue (Charlier et al., 2013; Stockstill-Cahill et al., 2012). For example, if magmatic processes have concentrated S on Mercury's surface, then perhaps Mercury's bulk silicate S concentration is substantially lower and can be consistent with the oxygen fugacity conditions needed to have 1–4 wt% Fe in the silicate.

On the other hand, if Mercury's surface Fe and S concentrations are similar to the planet's bulk silicate composition, then wt% levels of both Fe and S may be difficult to produce in a single metal–silicate core formation process as they require different oxygen fugacity conditions; to produce wt% levels of Fe in the silicate, conditions may not be reducing enough to keep a wt% level of S in the silicate rather than have it segregate into the metallic core. Studies of Earth's core formation have suggested the possibility of changing oxidation conditions during a prolonged period of core formation, with accreting material starting as highly reduced and becoming more oxidizing toward the end of accretion (Wade and Wood, 2005; Wood et al., 2006). Core formation on Mercury may have been more complicated as well. Additionally, the role of any late accretion, which may have added material to Mercury after the core had formed that could be incorporated into the planet's mantle, is unknown and, if it was sizable, could affect the planet's bulk silicate composition.

Another possibility is that the Fe measured on Mercury's surface has a large exogenic component, delivered to the surface from meteoritic materials but not mixed efficiently into the mantle. Mercury's proximity to the Sun results in a high flux of materials to its surface (Cintala, 1992), and it has been suggested that as much as 1–5 wt% FeO may be delivered to Mercury's surface by meteorites (Noble and Pieters, 2003). Other elements would be delivered as well, but the addition of Mg, Si, Al, etc. at even a few wt% is within the scatter of MESSENGER measurements (Nittler et al., 2011; Weider et al., 2012). If 1–5 wt% FeO on Mercury's surface was due to the delivery of exogenic meteoritic materials, that alone could be responsible for the 1–4 wt% Fe measured on Mercury's surface, implying that Mercury's surface rocks are actually almost entirely Fe-free. Such a result would be consistent with our experiments, which produce silicates with wt% levels of S but with Fe well below 1 wt%. Future geochemical measurements by MESSENGER, in particular the mapping of Fe abundances on Mercury's surface, have the potential to place important constraints on the amount and nature of any exogenic addition to Mercury's surface.

The silicate composition in our experiments was selected to be similar to MESSENGER measurements of Mercury's surface but also became highly enriched in Al during the runs due to being conducted in alumina capsules. Thus, the silicate composition of our experiments, reported in Table 1, is most certainly not Mercury's bulk silicate composition. Previous work has found that the silicate composition can affect the partitioning behavior of S (Haughton et al., 1974). Our experimental silicate composition is generally FeO-poor, such as observed for Mercury, and constant. The set of experiments conducted with the same starting composition but held for different run durations of 2–16 hours (#M1, #M31, and #M34) still produced similar silicate melt compositions. Of the 19 experiments, only three runs resulted in >1 wt% Fe being incorporated into the silicates. In these cases, the silicates contain ⩾13 wt% Fe and also have the lowest levels of S. While a different silicate composition might change the partitioning behavior of S, the combined metallic composition and oxygen fugacity effect that

is investigated systematically in this study would still be relevant. The single, FeO-poor silicate composition that we used here was chosen to be relevant to Mercury, but additional examination into the effects of different silicate compositions is worthwhile.

While our experiments begin to explore partitioning during core formation at Mercury, they are not perfect analogs of core formation on that planet. Our experiments were conducted at 1 atm and 1500 °C, and Mercury's core formation is expected to have occurred a higher pressures and temperatures. However, Mercury's core–mantle boundary is only at a pressure of ~5.5 GPa (Hauck et al., 2013), which limits the pressures and temperatures of possible core formation. Experimental studies examining the solubility of S in silicates in metal–silicate systems have found that S partitioning into silicate decreases with increasing pressure and increases with increasing temperature (Holzheid and Grove, 2002; Li and Agee, 2001; Rose-Weston et al., 2009). Thus, results from previous experimental studies suggest that the effects of increasing both pressure and temperature may offset one another, and that the partitioning behavior observed at 1 atm and 1500 °C may be applicable to higher pressure and temperature conditions. Nevertheless, experiments at higher pressures and temperatures are worthwhile.

One theory to explain Mercury's unusually large metallic core is that a giant impact removed a significant amount of silicate material (Benz et al., 2007). In this case, core formation would have initially occurred on a much larger planetary body and likely under conditions of higher pressure and temperature, not limited by the ~5.5 GPa of Mercury's current day core–mantle boundary. However, the energy required in a giant impact event to remove a significant amount of silicate material could also create significant melting in the remaining planet and thus potentially initiate a new set of core formation conditions in the smaller planetary body.

Overall, additional studies to determine Mercury's mantle and bulk silicate composition, to investigate effects of pressure, temperature, and silicate composition, and to map the distribution of Fe on Mercury's surface are likely to provide further insight into interpreting the 1–4 wt% of both S and Fe on Mercury's surface. Our results here indicate that it may be difficult to produce both Fe and S at wt% levels in Mercury's bulk silicate composition through a single-stage metal–silicate core-formation event.

3.2. Metal composition

Fig. 3 shows that the weight ratio metal/silicate partition coefficient for S, $D(S)$, in our experiments is well characterized as a function of the Si content of the metallic liquid. This general result is consistent with previous work that has shown the solubility of S increases in a silicate melt as conditions become more reducing, as discussed in the previous section. Our experiments vary both the oxygen fugacity of the run and the metallic composition, though these two parameters are related; as a system becomes more reducing, more Si will partition into the metallic phase (Kilburn and Wood, 1997). Metal–silicate experimental studies often estimate the oxygen fugacity conditions of a run relative to the iron–wüstite (IW) buffer by using the molar concentrations of Fe and FeO in the metal and silicate and either assuming that the activity coefficients are unity (Hillgren et al., 1994) or calculating the activity coefficients via a thermodynamically-based model (Wade and Wood, 2005; Wade et al., 2012). The further the metallic composition is from pure Fe, such as the Fe–S–Si metals in our experiments, the more important it can be to include a non-unity activity coefficient for Fe. For our experiments, we used the Metal Activity Calculator (www.earth.ox.ac.uk/~expet/metalact) after the model of Wade and Wood (2005) to determine the activity coefficient for Fe in our runs and assumed that the activity coefficient for FeO in the silicate was unity. We calculate that the oxygen fugacity varies in our set of experiments from roughly −1 to −6 ΔIW (log units below the iron–wüstite buffer), with the large majority of the runs below −4 ΔIW. This range of oxygen fugacities for our runs with wt% levels of S in the silicate melt is consistent with the calculated range of −4.5 to −7.3 ΔIW for Mercury's S-bearing magmas by Zolotov et al. (2013).

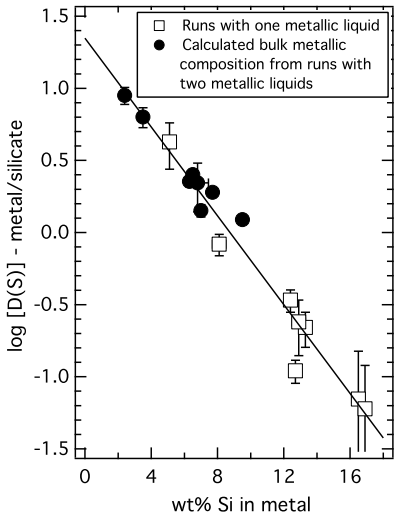

Fig. 3. The metal–silicate partition coefficient, $D(S)$, in our experiments is well fit as a function of the Si content of the metal. The best fit line is given in Eq. (1). Error bars are two standard deviations.

The results in Fig. 3 are plotted as a function of the Si content of the metal rather than as a function of the oxygen fugacity to avoid propagating any errors introduced by calculating the oxygen fugacity from the experiments. Even though our metallic phase is often S and Si-bearing, the uncertainty due to the activity coefficient model is not the major source of error in calculating oxygen fugacity. Rather, the largest uncertainty in our estimation of the oxygen fugacity in our runs is the very low FeO content of the silicate melt of the majority of the experiments. The Si content of the metal, which is present at wt% levels, is much better determined than the Fe content of the silicate, which is well below 1 wt% for most of the runs. We are interested in applying the S partitioning results to constrain the composition of the metal. Thus, parameterizing our results as a function of the Si content of the metal, as shown in Fig. 3, accomplishes this directly, and our data are well fit with this approach.

The equation of the fit in Fig. 3 is:

$$\log[D(S)] = 1.35 - 0.15[\text{wt\% Si}_{\text{metal}}] \quad (1)$$

Substituting the S contents of the metal and silicate for $D(S)$ in the above equation enables a relationship to be created between the S and Si content of the metal with a dependency on the S content of the silicate:

$$\log[\text{wt\% S}_{\text{metal}}] = 1.35 - 0.15[\text{wt\% Si}_{\text{metal}}] + \log[\text{wt\% S}_{\text{silicate}}] \quad (2)$$

4. Discussion

4.1. Mercury's core composition and evolution

Our experiments vary the metallic composition in the starting materials and produce final silicate compositions with S contents that range from <0.1 wt% to >8 wt%. Thus the S content of the silicate can place an important constraint on the metallic composition, if the S content was set through a metal–silicate equilibrium process.

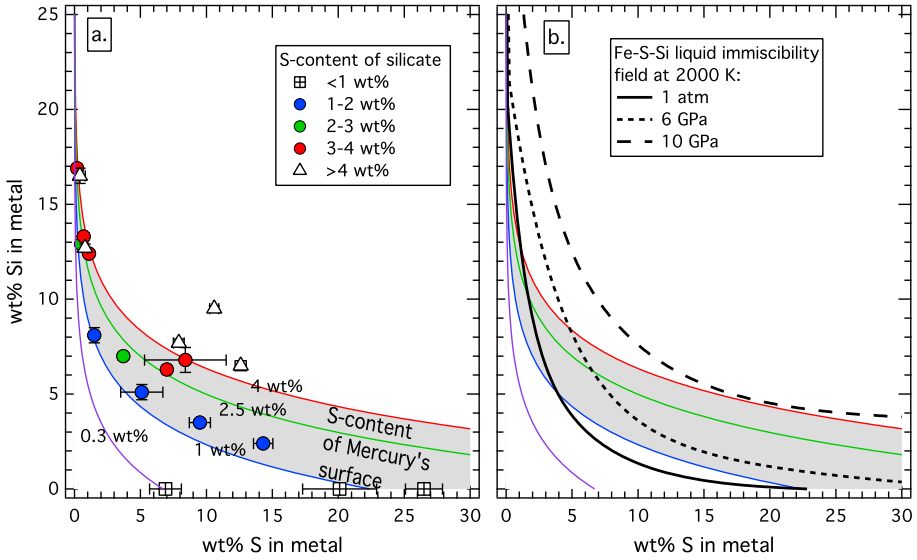

Fig. 4. (a) The shaded region denotes combinations of S and Si in the metal that are consistent with producing 1–4 wt% S in the silicate, as measured for Mercury's surface. The shaded region is calculated from Eq. (2), and the curves for four specific silicate S content values are shown (0.3, 1, 2.5, and 4 wt% S in the silicate). Eq. (2) was derived from fitting the experiments, which are also shown with two standard deviation error bars to evaluate the derived expression. (b) The same shaded region is shown with the liquid immiscibility field in the Fe–S–Si system at 2000 K and three pressures (Morard and Katsura, 2010). At a given pressure, compositions that are to the right of the liquid immiscibility field boundary will produce two liquids while compositions to the left will yield one liquid. Mercury's core–mantle boundary is ~5.5 GPa, and at that pressure, the more S-rich of the possible core combinations in the shaded region would fall within the liquid immiscibility field, resulting in two immiscible liquids, while those that are more Si-rich would not.

Fig. 4a graphs Eq. (2) for the range of 1–4 wt% S measured on Mercury's surface. Our experimental data, on which the equation is based, are also plotted. If Mercury's bulk silicate S content is between 1 and 4 wt% and that bulk silicate S content was set by metal–silicate differentiation, then the shaded region in Fig. 4a represents the possible S and Si combinations in Mercury's core that are consistent with that range of S contents. The discussion in the previous section is also relevant to the results shown here; differences between the pressure, temperature, and silicate composition of our experiments in comparison to core formation on Mercury could alter the position of the shaded region in Fig. 4a. However, the effects captured in Fig. 4a would still be relevant and any pressure, temperature, or silicate composition effect would be expected to shift the location of the shaded region while the overall functional form and shape of the shaded region would be expected to remain similar.

The overall features of Fig. 4a are consistent with previous work on the metal–silicate partitioning behavior of S. Having more Si partition into the metal requires more reducing conditions, and under more reducing conditions, S will partition more readily into the silicate (Kilburn and Wood, 1997). Thus as more Si goes into the metallic core, more S will partition into the silicate. As one example, if Mercury's core has a high Si content of ~10 wt%, then the S content of the core will be low, ~2 wt%, as S will partition almost equally between the silicate and the metal at these conditions. In contrast, if the core is richer in S with ~10 wt%, then the partition coefficient, $D(S)$, can be lower and the conditions less reducing, with less Si in the metal, and still result in 1–4 wt% S in the silicate. However, the combination of 10 wt% of both Si and S in the metal would result in a S content in the silicate significantly higher than the 1–4 wt% measured on Mercury's surface. Thus the shaded region in Fig. 4a provides constraints on possible Si and S core combinations that would produce 1–4 wt% S in Mercury's bulk silicate.

Our expression parameterizes the S content of the metal as a function of the Si content of the metal, and thus is not appropriate for Si-free metal systems. Our results in Fig. 4a indicate that to produce a bulk silicate with >1 wt% S, the metal must be either Si-bearing or contain >20 wt% S. The implication for Mercury is that if Mercury's bulk silicate composition has >1 wt% S, then Mercury's core is likely to contain Si. For moderate S contents in the metal, our results suggest that to have wt% levels of S in the silicate, there must be wt% levels of Si in the metal.

If the S on Mercury's surface is enriched relative to the bulk silicate planet, the requirement to have Si in the core is weakened. As an example, also plotted in Fig. 4a is a line showing the S and Si combinations needed to match 0.3 wt% S in the bulk silicate. Our results suggest that Si-free cores that contain >7 wt% S can produce bulk silicate combinations with 0.3 wt% S. Future work to better understand the relationship to between Mercury's surface and mantle compositions will provide important insight into this issue (Charlier et al., 2013; Stockstill-Cahill et al., 2012).

Additional constraints on Mercury's core composition can be provided by geophysical studies. Mercury's moment of inertia, as determined by data for Mercury's spin state and gravity field (Margot et al., 2012), can be used to constrain the core size and density, which can provide insight into the core's light element content. Hauck et al. (2013) ran several Monte Carlo models to investigate possible core compositions for Mercury in the Fe–S–Si system and concluded that a wide range of core compositions with either S or Si or both were consistent with the geophysical constraints. Thus, the model results were not able to distinguish between the possible compositions for the metallic core, with the exception of ruling out Si-free cores with <6 wt% S. Based on these results, Hauck et al. (2013) concluded that a substantial fraction of light element is present in Mercury's core that likely includes Si and possibly also S, and that in the Fe–S–Si system, a FeS-rich layer could form at the top of the core. Our results in Fig. 4 show a range of Si and S compositions that would be consistent with Mercury's moment of inertia based on the modeling results of Hauck et al. (2013).

Mercury's surface shows extensive lobate scarps believed to have formed by global contraction of the planet (Watters et al., 1998). Thermal models have shown global contraction can be tied to the cooling of the planet and place constraints on the crystallization history, and hence composition, of the core. Geophysical models based on explaining 1–2 km of radial contraction since the end of late heavy bombardment (Watters et al., 1998, 2009) con-

cluded that Mercury's core S content must be > ~6 wt% (Grott et al., 2011; Hauck et al., 2004). In contrast, Rivoldini et al. (2009) concluded that to have a solid inner core, <5 wt% S must be present in Mercury's core. However, all of these models only considered S as a light element in Mercury's core. The amount and identity of the light element in the core has a significant effect on the temperature at which crystallization will begin, with S depressing the crystallization temperature more significantly than Si (Raghavan, 1988). Additionally, a new estimate of Mercury's global contraction based on MESSENGER images suggests a potentially larger radius decrease of ~3–5 km (Di Achille et al., 2012). Future thermal models that incorporate a potential Fe–S–Si metallic core and use the latest estimates for Mercury's global radial contraction have the potential to provide additional constraints on Mercury's core composition.

Lastly, Mercury has a magnetic field that is consistent with being generated by an internal core dynamo (Anderson et al., 2011; Ness et al., 1975). The identity and concentration of the core's light element will influence the extent of compositional convection that is generated when a buoyant light element is excluded from the crystallizing solid inner core. Mercury's core–mantle boundary pressure is ~5.5 GPa, and the central core pressure is ~36 GPa (Hauck et al., 2013). Even at 25 GPa, S is effectively excluded from the crystallizing Fe metal (Li et al., 2001), making it an efficient light element to drive compositional convection. In contrast, Si partitions nearly equally into the crystallizing solid Fe and the residual metallic liquid even at a pressure of 21 GPa (Kuwayama and Hirose, 2004), which would be much less effective at driving compositional convection. The weakness of Mercury's magnetic field has been a challenge for modeling its generation from an internal dynamo, leading to suggestions of S-bearing cores with different precipitation zones (Vilim et al., 2010) or low core S contents to minimize compositional convection (Manglik et al., 2010). However, the models to date have not considered the generation of Mercury's dynamo in the Fe–S–Si system, and perhaps the presence of Si as an important light element in Mercury's core could reduce compositional convection in a manner consistent with the observed magnetic field strength. Overall, the existence of Mercury's internally driven magnetic field has the potential to provide additional constraints on Mercury's core composition.

Related to Mercury's internal dynamo generation and the global contraction of the planet is the evolution and crystallization of the core. Fig. 4b compares the range of core Si and S contents suggested by our experiments with the liquid immiscibility field in the Fe–S–Si at 2000 K and different pressures (Morard and Katsura, 2010). As the pressure increases, the liquid immiscibility field decreases. At Mercury's core–mantle boundary pressure of ~5.5 GPa (Hauck et al., 2013), the range of S and Si contents suggested by our experiments fall both within and outside the liquid immiscibility field. By 10 GPa, the liquid immiscibility field has decreased to the extent that none of the S and Si combinations suggested by our experiments would initially encounter liquid immiscibility. Mercury's central core pressure is ~36 GPa (Hauck et al., 2013), and, thus, the majority of Mercury's core would not be expected to initially encounter liquid immiscibility except potentially near the core–mantle boundary. However, encountering liquid immiscibility and forming a Si-rich liquid and a S-rich liquid could facilitate the creation of a S-rich layer at the base of the mantle. A S-rich layer at the base of the mantle could eventually crystallize and form a solid FeS layer, as has been considered (Hauck et al., 2013; Smith et al., 2012). Additionally, as the core crystallizes, any S will become enriched in the liquid, and thus though the bulk core composition might not experience liquid immiscibility initially, its composition could evolve into the liquid immiscibility field as crystallization proceeds. If Mercury's core contains both Si and S, a variety of evolutionary scenarios are possible and can be explored in more detail with future models.

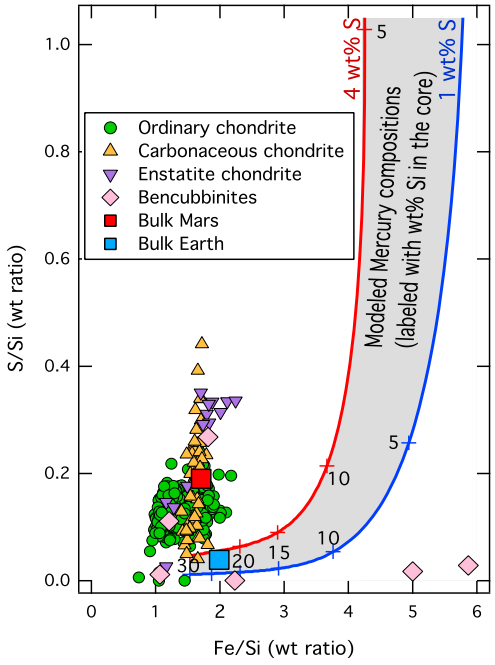

Fig. 5. The shaded region shows Mercury's bulk Fe/Si and S/Si ratios as calculated by using the range of possible core compositions in the Fe–S–Si system from Fig. 4. The majority of possible core compositions produce bulk Mercury values that differ significantly from primitive meteorites or estimates for bulk Earth (McDonough, 2003) or bulk Mars (Dreibus and Wanke, 1985), though core compositions with extreme amounts of Si of ~25 wt% produce Fe/Si and S/Si ratios that resemble those of bulk Earth. Meteorite data compiled in Nittler et al. (2000). Bencubbinite data from Jarosewich (1990) and Lauretta et al. (2007).

4.2. Mercury's bulk composition

With an estimate of the composition of Mercury's large core, we can estimate the bulk Fe, S, and Si contents of the planet as a whole, using a core fraction of 0.67 (Anderson et al., 1987). For Mercury's bulk silicate composition, we used a composition with no Fe, 25 wt% Si, and 1–4 wt% S, similar to MESSENGER's measurements of Mercury's surface (Evans et al., 2012; Nittler et al., 2011; Starr et al., 2012; Weider et al., 2012); including 1–4 wt% Fe in the silicate has a negligible effect on the estimations, since Mercury's large core is the major source of the planet's bulk Fe composition. For Mercury's core, the S and Si content ranges shown in Fig. 4 were used along with 5 wt% Ni and the remainder of the composition composed of Fe. Fig. 5 plots the resulting range of Mercury's bulk composition on a plot of the S/Si weight ratio against the Fe/Si weight ratio. The two bounding model lines for Mercury's bulk composition with 1 or 4 wt% S in the silicate are also labeled with points that correspond to the wt% Si in Mercury's core, to ease the comparison to Fig. 4.

Fig. 5 also plots the bulk compositions of ordinary, carbonaceous, and enstatite chondrites, as compiled and labeled as "whole rock" values by Nittler et al. (2000) and applied to compositional measurements of the asteroid Eros (Nittler et al., 2001). Estimates of the compositions of bulk Earth (McDonough, 2003) and bulk Mars (Dreibus and Wanke, 1985) are also plotted, as are the few bulk compositions available for bencubbinite meteorites (Jarosewich, 1990; Lauretta et al., 2007). From Fig. 5 it is clear that the large majority of estimated bulk compositions of Mercury from our experiments differ significantly from primitive meteorite compositions. Bencubbinites, suggested as potentially relevant composition for Mercury's building blocks (Brown and Elkins-Tanton,

2009), also do not provide a good match, though they display considerable compositional heterogeneity on the sample size analyzed. The difference between Mercury's bulk compositions and primitive meteorites has been a known issue ever since Mercury's unusually high density was discovered. Our new work to constrain Mercury's core composition only shows that even with improved constraints on the core composition, Mercury's bulk composition is very different than Earth, Mars, or the meteorites in our collections. This could imply that either Mercury formed from different starting materials, due to a range of hypothesized processes (Taylor and Scott, 2003) or that a giant impact stripped much of Mercury's silicate away, making the current day Mercury just a remnant of a once larger body (Benz et al., 2007).

Fig. 5 does show one alternative to these formation scenarios. If Mercury's core contains ~25 wt% Si, then the bulk composition is very close to that of the Earth for its estimated S/Si and Fe/Si weight ratios. Examining Fig. 4 shows that the range of possible core compositions with 25 wt% Si is extrapolated beyond our experimental data and implies an essentially S-free core. While an extremely Si-rich core could reconcile Mercury's bulk Fe/Si ratio with common primitive meteorites, the partitioning of such a large amount of Si into the core would leave Mercury's bulk silicate with highly elevated values for the ratios of other elements, including Mg/Si, Al/Si, and Ca/Si. MESSENGER's chemical data are limited to surface measurements, but future work that seeks to estimate Mercury's mantle and bulk silicate composition from the measured surface compositional values thus also has the potential to constrain the amount of Si in Mercury's core by determining these ratios. Additionally, it is not clear if 25 wt% Si in the core would be consistent with Mercury's moment of inertia constraints or thermal models of the planet and a partially molten core. The convection and dynamo generation in a Si-rich, S-free core has not been widely considered. Additionally, a core with 25 wt% Si would imply extremely reducing conditions, replacing the issue of Mercury's bulk composition with the question of how did Mercury form under such reducing conditions in comparison to other planetary bodies. Overall, Mercury's bulk composition remains unique in comparison to other planetary materials and is an important clue to unraveling the secrets of the planet's formation.

5. Summary and conclusions

Our experimental study systematically examined metal–silicate equilibrium partitioning under a range of oxygen fugacity and metallic composition conditions. If Mercury's surface composition is representative of the planet's bulk silicate composition and if the planet experienced metal–silicate equilibrium during formation of its core, then a few key conclusions can be drawn from our results:

1. Mercury's surface composition with 1–4 wt% of both Fe and S is not compatible with being formed by simple metal–silicate equilibrium, as the reducing conditions needed to partition S into the silicate will deplete the silicate in Fe. This could indicate that Mercury's surface is not representative of the bulk silicate planet, that core formation was more complicated than a single stage metal–silicate processes, that a significant amount of material was added to Mercury's mantle during late accretion after core formation, that our experiments are lacking as analogs for Mercury due to differences in pressure, temperature, or compositions, or that a significant component of Mercury's surface Fe was delivered by meteorites.
2. Mercury's core composition can be constrained to a range of combinations in the Fe–S–Si system based on the requirement of 1–4 wt% S in the silicate. For core S contents $<$20 wt%, Mercury's core must contain Si. For core Si contents $>$10 wt%, Mercury's core has $<$2 wt% S. As the core Si content increases, the core S content decreases, as more S partitions into the silicate.
3. Mercury's bulk Fe, S, and Si compositions can be estimated by using our newly determined constraints on the composition of the planet's large core. For the large majority of the Fe–S–Si core combinations, Mercury's bulk Fe/Si and S/Si ratios differ greatly from primitive meteorites and the bulk Earth or bulk Mars. However, a S-free core with ~25 wt% Si can produce a bulk Mercury composition that resembles that of the bulk Earth for Fe/Si and S/Si ratios, though such a large core Si content raises additional issues and has implications for the planet's Mg/Si and other elemental ratios. Alternatively, Mercury's unusual bulk composition may indicate that the current planet is only a portion of what it once was, with a sizable component stripped off by a giant impact event.

Overall, one of the main conclusions to be drawn from this study is that such experimental work can provide constraints on the composition of Mercury's core. The work presented here is just the beginning of experimental studies to investigate Mercury's core and the planet as a whole. Future metal–silicate studies examining the effects of pressure, temperature, and composition are worthwhile. Work to interpret Mercury's surface composition in the context of the planet's mantle and bulk silicate composition is also well motivated. Geophysical and thermal evolution models of Mercury's interior that examine cores in the Fe–S–Si system may provide new constraints on the core composition, as may models to generate Mercury's internal magnetic field. Additionally, MESSENGER is continuing to orbit Mercury and has the potential to return new data through early 2015, undoubtedly leading to new insights about the Solar System's innermost planet.

Acknowledgements

This work was supported by NASA Cosmochemistry grant NNX12AH88G. The Student Research Participation Program at APL is administered by the Oak Ridge Institute for Science and Education. We thank John Armstrong for masterful advice and guidance during the SEM analyses, and the Geophysical Laboratory of the Carnegie Institution of Washington for providing access to the analytical facilities. We thank two anonymous reviewers and Editor Tim Elliott for comments that served to improve the final manuscript.

Appendix A. Supplementary material

Supplementary material related to this article can be found online at http://dx.doi.org/10.1016/j.epsl.2014.01.004.

References

Anderson, J.D., Colombo, G., Esposito, P.B., Lau, E.L., Trager, G.B., 1987. The mass, gravity-field, and ephemeris of Mercury. Icarus 71, 337–349.

Anderson, B.J., Johnson, C.L., Korth, H., Purucker, M.E., Winslow, R.M., Slavin, J.A., Solomon, S.C., McNutt Jr., R.L., Raines, J.M., Zurbuchen, T.H., 2011. The global magnetic field of Mercury from MESSENGER orbital observations. Science 333, 1859–1862.

Bedini, P.D., Solomon, S.C., Finnegan, E.J., Calloway, A.B., Ensor, S.L., McNutt, R.L., Anderson, B.J., Prockter, L.M., 2012. MESSENGER at Mercury: A mid-term report. Acta Astronaut. 81, 369–379.

Benz, W., Anic, A., Horner, J., Whitby, J.A., 2007. The origin of Mercury. Space Sci. Rev. 132, 189–202.

Berthet, S., Malavergne, V., Righter, K., 2009. Melting of the Indarch meteorite (EH4 chondrite) at 1 GPa and variable oxygen fugacity: Implications for early planetary differentiation processes. Geochim. Cosmochim. Acta 73, 6402–6420.

Blewett, D.T., Lucey, P.G., Hawke, B.R., Ling, G.G., Robinson, M.S., 1997. A comparison of Mercurian reflectance and spectral quantities with those of the Moon. Icarus 129, 217–231.

Brown, S.M., Elkins-Tanton, L.T., 2009. Compositions of Mercury's earliest crust from magma ocean models. Earth Planet. Sci. Lett. 286, 446–455.
Chabot, N.L., Saslow, S.A., McDonough, W.F., McCoy, T.J., 2007. The effect of Ni on element partitioning during iron meteorite crystallization. Meteorit. Planet. Sci. 42, 1735–1750.
Chabot, N.L., Saslow, S.A., McDonough, W.F., Jones, J.H., 2009. An investigation of the behavior of Cu and Cr during iron meteorite crystallization. Meteorit. Planet. Sci. 44, 505–519.
Chabot, N.L., Safko, T.M., McDonough, W.F., 2010. Effect of silicon on trace element partitioning in iron-bearing metallic melts. Meteorit. Planet. Sci. 45, 1243–1257.
Charlier, B., Grove, T.L., Zuber, M.T., 2013. Phase equilibria of ultramafic compositions on Mercury and the origin of the compositional dichotomy. Earth Planet. Sci. Lett. 363, 50–60.
Chen, B., Li, J., Hauck, S.A., 2008. Non-ideal liquidus curve in the Fe–S system and Mercury's snowing core. Geophys. Res. Lett. 35.
Cintala, M.J., 1992. Impact-induced thermal effects in the lunar and mercurian regoliths. J. Geophys. Res., Planets 97, 947–973.
Di Achille, G., Popa, C., Massironi, M., Epifani, E.M., Zusi, M., Cremonese, G., Palumbo, P., 2012. Mercury's radius change estimates revisited using MESSENGER data. Icarus 221, 456–460.
Dreibus, G., Wanke, H., 1985. Mars, a volatile-rich planet. Meteoritics 20, 367–381.
Evans, L.G., Peplowski, P.N., Rhodes, E.A., Lawrence, D.J., McCoy, T.J., Nittler, L.R., Solomon, S.C., Sprague, A.L., Stockstill-Cahill, K.R., Starr, R.D., Weider, S.Z., Boynton, W.V., Hamara, D.K., Goldsten, J.O., 2012. Major-element abundances on the surface of Mercury: Results from the MESSENGER gamma-ray spectrometer. J. Geophys. Res. 117, E00L07. http://dx.doi.org/10.1029/2012JE004178.
Goettel, K.A., 1988. Present bounds on the bulk composition of Mercury – implications for planetary formation processes. In: Vilas, F., Chapman, C.R., Matthews, M.S. (Eds.), Mercury. University of Arizona Press, Tucson, AZ, pp. 613–621.
Grott, M., Breuer, D., Laneuville, M., 2011. Thermo-chemical evolution and global contraction of Mercury. Earth Planet. Sci. Lett. 307, 135–146.
Hauck, S.A., Dombard, A.J., Phillips, R.J., Solomon, S.C., 2004. Internal and tectonic evolution of Mercury. Earth Planet. Sci. Lett. 222, 713–728.
Hauck, S.A., Margot, J.-L., Solomon, S.C., Phillips, R.J., Johnson, C.L., Lemoine, F.G., Mazarico, E., McCoy, T.J., Padovan, S., Peale, S.J., Perry, M.E., Smith, D.E., Zuber, M.T., 2013. The curious case of Mercury's internal structure. J. Geophys. Res., Planets 118, 1204–1220.
Haughton, D.R., Roeder, P.L., Skinner, B.J., 1974. Solubility of sulfur in mafic magmas. Econ. Geol. 69, 451–467.
Hillgren, V.J., Drake, M.J., Rubie, D.C., 1994. High-pressure and high-temperature experiments on core–mantle segregation in the accreting Earth. Science 264, 1442–1445.
Holzheid, A., Grove, T.L., 2002. Sulfur saturation limits in silicate melts and their implications for core formation scenarios for terrestrial planets. Am. Mineral. 87, 227–237.
Jarosewich, E., 1990. Chemical-analyses of meteorites – a compilation of stony and iron meteorite analyses. Meteoritics 25, 323–337.
Keil, K., 1989. Enstatite meteorites and their parent bodies. Meteoritics 24, 195–208.
Kilburn, M.R., Wood, B.J., 1997. Metal–silicate partitioning and the incompatibility of S and Si during core formation. Earth Planet. Sci. Lett. 152, 139–148.
Kuwayama, Y., Hirose, K., 2004. Phase relations in the system Fe–FeSi at 21 GPa. Am. Mineral. 89, 273–276.
Lauretta, D.S., Goreva, J.S., Hill, D.H., Killgore, M., 2007. Bulk compositions of the CB chondrites, Bencubbin, Fountain Hills, MAC 02675, and MIL 05082. In: 38th Lunar and Planetary Science Conference. League City, Texas, p. 2236 (No. 1338).
Li, J., Agee, C.B., 2001. Element partitioning constraints on the light element composition of the Earth's core. Geophys. Res. Lett. 28, 81–84.
Li, J., Fei, Y., Mao, H.K., Hirose, K., Shieh, S.R., 2001. Sulfur in the Earth's inner core. Earth Planet. Sci. Lett. 193, 509–514.
Malavergne, V., Toplis, M.J., Berthet, S., Jones, J., 2010. Highly reducing conditions during core formation on Mercury: Implications for internal structure and the origin of a magnetic field. Icarus 206, 199–209.
Manglik, A., Wicht, J., Christensen, U.R., 2010. A dynamo model with double diffusive convection for Mercury's core. Earth Planet. Sci. Lett. 289, 619–628.
Margot, J.L., Peale, S.J., Jurgens, R.F., Slade, M.A., Holin, I.V., 2007. Large longitude libration of Mercury reveals a molten core. Science 316, 710–714.
Margot, J.L., Peale, S.J., Solomon, S.C., Hauck, S.A., Ghigo, F.D., Jurgens, R.F., Yseboodt, M., Giorgini, J.D., Padovan, S., Campbell, D.B., 2012. Mercury's moment of inertia from spin and gravity data. J. Geophys. Res., Planets 117.
McClintock, W.E., Izenberg, N.R., Holsclaw, G.M., Blewett, D.T., Domingue, D.L., Head, J.W., Helbert, J., McCoy, T.J., Murchie, S.L., Robinson, M.S., Solomon, S.C., Sprague, A.L., Vilas, F., 2008. Spectroscopic observations of Mercury's surface reflectance during MESSENGER's first Mercury flyby. Science 321, 62–65.
McCoy, T.J., Dickinson, T.L., Lofgren, G.E., 1999. Partial melting of the Indarch (EH4) meteorite: A textural, chemical, and phase relations view of melting and melt migration. Meteorit. Planet. Sci. 34, 735–746.
McCubbin, F.M., Riner, M.A., Vander Kaaden, K.E., Burkemper, L.K., 2012. Is Mercury a volatile-rich planet? Geophys. Res. Lett. 39, L09202.
McDonough, W.F., 2003. Compositional model for the Earth's core. In: Carlson, R.W. (Ed.), Treatise on Geochemistry. Elsevier, pp. 547–568.
Morard, G., Katsura, T., 2010. Pressure–temperature cartography of Fe–S–Si immiscible system. Geochim. Cosmochim. Acta 74, 3659–3667.
Ness, N.F., Behannon, K.W., Lepping, R.P., Whang, Y.C., 1975. Magnetic-field of Mercury. 1. J. Geophys. Res., Space 80, 2708–2716.
Nittler, L.R., Clark, P.E., McCoy, T.J., Murphy, M.E., Trombka, J.I., 2000. Bulk compositional trends in meteorites: a guide for analysis and interpretation of NEAR XGRS data from asteroid 433 Eros. In: 31st Annual Lunar and Planetary Science Conference. Houston, Texas, p. 1711.
Nittler, L.R., Starr, R.D., Lim, L., McCoy, T.J., Burbine, T.H., Reedy, R.C., Trombka, J.I., Gorenstein, P., Squyres, S.W., Boynton, W.V., McClanahan, T.P., Bhangoo, J.S., Clark, P.E., Murphy, M.E., Killen, R., 2001. X-ray fluorescence measurements of the surface elemental composition of asteroid 433 Eros. Meteorit. Planet. Sci. 36, 1673–1695.
Nittler, L.R., Starr, R.D., Weider, S.Z., McCoy, T.J., Boynton, W.V., Ebel, D.S., Ernst, C.M., Evans, L.G., Goldsten, J.O., Hamara, D.K., Lawrence, D.J., McNutt Jr., R.L., Schlemm 2nd, C.E., Solomon, S.C., Sprague, A.L., 2011. The major-element composition of Mercury's surface from MESSENGER X-ray spectrometry. Science 333, 1847–1850.
Noble, S.K., Pieters, C.M., 2003. Space weathering on Mercury: Implications for remote sensing. Sol. Syst. Res. 37, 31–35.
Peplowski, P.N., Evans, L.G., Hauck 2nd, S.A., McCoy, T.J., Boynton, W.V., Gillis-Davis, J.J., Ebel, D.S., Goldsten, J.O., Hamara, D.K., Lawrence, D.J., McNutt Jr., R.L., Nittler, L.R., Solomon, S.C., Rhodes, E.A., Sprague, A.L., Starr, R.D., Stockstill-Cahill, K.R., 2011. Radioactive elements on Mercury's surface from MESSENGER: implications for the planet's formation and evolution. Science 333, 1850–1852.
Peplowski, P.N., Lawrence, D.J., Rhodes, E.A., Sprague, A.L., McCoy, T.J., Denevi, B.W., Evans, L.G., Head, J.W., Nittler, L.R., Solomon, S.C., Stockstill-Cahill, K.R., Weider, S.Z., 2012a. Variations in the abundances of potassium and thorium on the surface of Mercury: Results from the MESSENGER gamma-ray spectrometer. J. Geophys. Res. 117, E00L04.
Peplowski, P.N., Rhodes, E.A., Hamara, D.K., Lawrence, D.J., Evans, L.G., Nittler, L.R., Solomon, S.C., 2012b. Aluminum abundance on the surface of Mercury: Application of a new background-reduction technique for the analysis of gamma-ray spectroscopy data. J. Geophys. Res. 117, E00L10.
Raghavan, V., 1988. Phase Diagrams of Ternary Iron Alloys. The Indian Institute of Metals, Calcutta.
Riner, M.A., Bina, C.R., Robinson, M.S., Desch, S.J., 2008. Internal structure of Mercury: Implications of a molten core. J. Geophys. Res., Planets 113, E08013.
Rivoldini, A., Van Hoolst, T., Verhoeven, O., 2009. The interior structure of Mercury and its core sulfur content. Icarus 201, 12–30.
Robinson, M.S., Taylor, G.J., 2001. Ferrous oxide in Mercury's crust and mantle. Meteorit. Planet. Sci. 36, 841–847.
Rose-Weston, L., Brenan, J.M., Fei, Y.W., Secco, R.A., Frost, D.J., 2009. Effect of pressure, temperature, and oxygen fugacity on the metal–silicate partitioning of Te, Se, and S: Implications for earth differentiation. Geochim. Cosmochim. Acta 73, 4598–4615.
Smith, D.E., Zuber, M.T., Phillips, R.J., Solomon, S.C., Hauck 2nd, S.A., Lemoine, F.G., Mazarico, E., Neumann, G.A., Peale, S.J., Margot, J.L., Johnson, C.L., Torrence, M.H., Perry, M.E., Rowlands, D.D., Goossens, S., Head, J.W., Taylor, A.H., 2012. Gravity field and internal structure of Mercury from MESSENGER. Science 336, 214–217.
Starr, R.D., Schriver, D., Nittler, L.R., Weider, S.Z., Byrne, P.K., Ho, G.C., Rhodes, E.A., Schlemm, C.E., Solomon, S.C., Travnicek, P.M., 2012. MESSENGER detection of electron-induced X-ray fluorescence from Mercury's surface. J. Geophys. Res., Planets 117, E00L02.
Stockstill-Cahill, K.R., McCoy, T.J., Nittler, L.R., Weider, S.Z., Hauck, S.A., 2012. Magnesium-rich crustal compositions on Mercury: Implications for magmatism from petrologic modeling. J. Geophys. Res., Planets 117, E00L15.
Taylor, G.J., Scott, E.R.D., 2003. Mercury. In: Davis, A.M. (Ed.), Treatise on Geochemistry, vol. 1. Elsevier, pp. 477–485.
Vilas, F., 1988. Surface composition of Mercury from reflectance spectrophotometry. In: Vilas, F., Chapman, C.R., Matthews, M.S. (Eds.), Mercury. University of Arizona Press, Tuscon, AZ, pp. 59–76.
Vilim, R., Stanley, S., Hauck, S.A., 2010. Iron snow zones as a mechanism for generating Mercury's weak observed magnetic field. J. Geophys. Res., Planets 115, E11003.
Wade, J., Wood, B.J., 2005. Core formation and the oxidation state of the Earth. Earth Planet. Sci. Lett. 236, 78–95.
Wade, J., Wood, B.J., Tuff, J., 2012. Metal–silicate partitioning of Mo and W at high pressures and temperatures: Evidence for late accretion of sulphur to the Earth. Geochim. Cosmochim. Acta 85, 58–74.
Wallace, P., Carmichael, I.S.E., 1992. Sulfur in basaltic magmas. Geochim. Cosmochim. Acta 56, 1863–1874.

Watters, T.R., Robinson, M.S., Cook, A.C., 1998. Topography of lobate scarps on Mercury: New constraints on the planet's contraction. Geology 26, 991–994.
Watters, T.R., Solomon, S.C., Robinson, M.S., Head, J.W., Andre, S.L., Hauck, S.A., Murchie, S.L., 2009. The tectonics of Mercury: The view after MESSENGER's first flyby. Earth Planet. Sci. Lett. 285, 283–296.
Weider, S.Z., Nittler, L.R., Starr, R.D., McCoy, T.J., Stockstill-Cahill, K.R., Byrne, P.K., Denevi, B.W., Head, J.W., Solomon, S.C., 2012. Chemical heterogeneity on Mercury's surface revealed by the MESSENGER X-ray spectrometer. J. Geophys. Res. 117, E00L05.
Wood, B.J., Walter, M.J., Wade, J., 2006. Accretion of the Earth and segregation of its core. Nature 441, 825–833.
Zolotov, M., Sprague, A.L., Hauck, S.A., Nittler, L., Solomon, S.C., Weider, S.Z., 2013. The redox state, FeO content, and origin of sulfur-rich magmas on Mercury. J. Geophys. Res. 118, 138–146.